

Quasinormal Ringing and Shadows of Black Holes and Wormholes in Dark Matter-Inspired Weyl Gravity

R. A. Konoplya,[†] A. Khrabustovskyi,[‡] Jan Kríž,[‡] A. Zhidenko^{*}

[†]Research Centre for Theoretical Physics and Astrophysics,
Institute of Physics, Silesian University in Opava,
Bezručovo náměstí 13, CZ-74601 Opava, Czech Republic

[‡]Department of Physics, Faculty of Science, University of Hradec Králové,
Rokitanského 62, 50003 Hradec Králové, Czech Republic

^{*}Centro de Matemática, Computação e Cognição (CMCC),
Universidade Federal do ABC (UFABC),
Rua Abolição, CEP: 09210-180, Santo André, SP, Brazil

E-mail: roman.konoplya@gmail.com, andrii.khrabustovskyi@uhk.cz,
jan.kriz@uhk.cz, olexandr.zhydenko@ufabc.edu.br

Abstract. Weyl gravity naturally generates effective dark matter and cosmological constant terms as integration constants, eliminating the need to explicitly introduce them into the theory. Additionally, the framework permits three intriguing solutions for compact objects: an asymptotically de Sitter Schwarzschild-like black hole described by the Mannheim-Kazanas solution, a non-Schwarzschild black hole, and a traversable wormhole that exists without exotic matter. In this work, we investigate the quasinormal spectra of all three solutions.

We demonstrate that when the mass of the black hole corresponding to the Mannheim-Kazanas solution approaches zero, the perturbation equations yield an exact solution expressible through hypergeometric functions. The quasinormal modes of black holes in Weyl gravity can be classified into three distinct branches: Schwarzschild-like modes modified by effective dark matter and cosmological terms, and modes associated with empty spacetime (de Sitter and dark matter branches), which are further influenced by the black hole mass. Previous studies have shown that the dark matter term induces a secondary stage of quasinormal ringing following the initial Schwarzschild phase. Here, we compute the frequencies using convergent methods and elucidate how this unique time-domain behavior translates into the frequency domain.

Furthermore, we demonstrate that the non-Schwarzschild black hole can be distinguished from both the Schwarzschild-like solution and the wormhole through their distinct quasinormal spectra. We also compute shadow radii for black holes and wormholes within Weyl gravity, revealing that wormholes with large throat radii can produce significantly smaller shadows compared to black holes of equivalent mass.

Contents

1	Introduction	1
2	Weyl Gravity and Mannheim-Kazanas solution	2
3	Jizba-Mudruška solution	4
4	Wavelike equations and effective potentials	6
5	Exact solutions in the limit of vanishing black-hole mass	8
5.1	Zero cosmological constant, $\gamma < 0$	8
5.2	Nonzero cosmological constant	9
6	Shadows	10
7	Numerical methods for the calculation of quasinormal modes	12
7.1	WKB approach	12
7.2	Time-domain integration	13
7.3	Bernstein polynomial method	14
8	Quasinormal modes	15
9	Conclusions	20

1 Introduction

The two major challenges of modern physics at large scales are explaining the accelerating separation of galaxies and the invisibility of the majority of cosmic matter within galaxies. These issues have been addressed through various, often artificial, approaches, such as introducing additional terms and parameters into Einstein's theory to replicate the observed effects. An elegant solution to both problems was proposed long ago by Mannheim and Kazanas in [1], where they demonstrated that pure Weyl gravity, without the Einstein term, admits a Schwarzschild-like solution incorporating effective cosmological and dark matter terms. Remarkably, these terms emerge naturally from the theory rather than being formally introduced as parameters or extra fields or distributions of matter. This is possible because the equations of motion in Weyl gravity are of fourth order, with four integration constants. Two of these constants can be associated with the dark matter and cosmological terms.

Furthermore, as recently shown in [2], pure Weyl gravity provides a solution to a third intriguing problem: the existence of traversable wormholes without requiring exotic matter. In Einstein's gravity, traversable wormholes necessitate various forms of exotic matter, such as phantom-like fields [3], or finely tuned Maxwell-Dirac systems [4, 5]. While the latter involves ordinary matter fields, it still violates traditional energy conditions. In contrast, Weyl gravity admits solutions for traversable wormholes [2] as well as for non-Schwarzschild-like black holes, which differ qualitatively from the original Schwarzschild-like Mannheim-Kazanas black hole solution [1].

One of the most important characteristics of a compact object is its quasinormal mode spectrum, which governs the evolution of perturbations around the object [6–8]. The boundary conditions for quasinormal modes of wormholes and black holes are fundamentally similar [9]. Consequently, in certain parameter ranges, a wormhole may mimic a black hole [10], though significant differences in their spectra [11] and the late-time evolution of perturbations [12, 13] may still exist. These distinctions make the study of perturbation evolution in Weyl gravity highly compelling.

Quasinormal modes of Schwarzschild-like Mannheim-Kazanas black holes have been investigated in a few studies [14–18]. However, only the Schwarzschild branch of modes has been analyzed in detail. Notably, as shown in [17], the evolution of perturbations in this context comprises three distinct stages, each dominated by a different branch of modes: the Schwarzschild stage, the dark matter stage, and the asymptotic de Sitter stage. A comprehensive analysis of these stages in the frequency domain is still lacking. Moreover, other solutions in Weyl gravity, such as traversable wormholes and non-Schwarzschild black holes [2], have not yet been studied in terms of their quasinormal spectra.

In this work, we address these gaps by studying the time-domain evolution of perturbations and the quasinormal frequency spectra of all branches for the following compact objects in Weyl gravity:

- (a) Mannheim-Kazanas black holes [1],
- (b) Non-Mannheim-Kazanas black holes [2],
- (c) Traversable wormholes [2].

We demonstrate that for a zero-mass Mannheim-Kazanas metric, perturbation equations in the empty space of Weyl gravity allow for an exact solution, with the quasinormal modes of empty space representing the appropriate limit of compact object modes as the mass approaches zero. Additionally, we reveal several peculiarities in the spectra of these objects, which differ significantly from the spectrum of Schwarzschild spacetime in Einstein gravity. In addition, we calculate the radius of the shadow cast by all three objects and show that wormholes can be clearly distinguished from black holes in this respect.

In Section 2, we outline the fundamentals of Weyl gravity and the Mannheim-Kazanas black hole solution. Section 3 provides a review of the Jizba-Mudruška solution, which encompasses two types of objects: a black hole distinct from the Mannheim-Kazanas solution and a wormhole. Section 4 introduces the perturbation equations and effective potentials, while Section 5 examines a special case where the mass of the Mannheim-Kazanas black hole vanishes, allowing for an exact solution. In Section 7, we discuss the numerical and semi-analytical methods used to determine the quasinormal frequencies. Finally, Section 8 analyzes the obtained quasinormal frequencies and the time-domain evolution of perturbations. Section 6 is devoted to calculations the shadows radii for these black holes and wormholes. The conclusions (Section 9) summarize our results.

2 Weyl Gravity and Mannheim-Kazanas solution

Within the framework of Weyl conformal gravity, the effective cosmological constant emerges naturally as an integration constant in the background solution to the vacuum field equations

[1]. The corresponding action is expressed as:

$$S = \int d^4x \sqrt{-g} C^{abcd} C_{abcd}, \quad (2.1)$$

where g denotes the determinant of the metric tensor and C_{abcd} is the conformal Weyl tensor,

$$C_{abcd} = R_{abcd} - \frac{1}{2} (R_{ac}g_{bd} + R_{bd}g_{ac} - R_{ad}g_{bc} - R_{bc}g_{ad}) + \frac{1}{6} R (g_{ac}g_{bd} - g_{ad}g_{bc}). \quad (2.2)$$

The equation of motion under varying the metric is expressed via the Bach tensor,

$$2\partial_a \partial_d C^{ac}{}_{bc} + R_{ad} C^{ac}{}_{bc} = 0.$$

Here R_{ab} is the Ricci tensor. Notably, Birkhoff's theorem holds true within Weyl conformal gravity [19]. A static and spherically symmetric vacuum solution representing a black hole in this theory was first derived in [1].

The Mannheim-Kazanas solution is a solution to the field equations derived from the conformal gravity action, which fundamentally differ from Einstein's equations. This solution was introduced by P. Mannheim and D. Kazanas in the context of efforts to explain galactic rotation curves without invoking dark matter. Unlike standard General Relativity, which relies on the Einstein-Hilbert action, conformal gravity is based on the Weyl action. The Weyl action is invariant under conformal transformations, meaning it remains unchanged under local rescaling of the metric $g_{\mu\nu}(x) \rightarrow \Omega^2(x)g_{\mu\nu}(x)$, where $\Omega(x)$ is a smooth, nonzero function of spacetime coordinates.

The Mannheim-Kazanas solution is a static, spherically symmetric metric derived from conformal gravity. The spacetime interval in this solution is [1]:

$$ds^2 = -f(r)dt^2 + \frac{dr^2}{f(r)} + R(r)^2 (d\theta^2 + \sin^2 \theta d\phi^2), \quad (2.3)$$

where the metric functions are given by:

$$f(r) = 1 - \alpha - \frac{2M}{r} + \gamma r - kr^2, \quad R(r) = r. \quad (2.4)$$

Since Mannheim and Kazanas considered the neutral black holes, the values of α and M are not independent and can be defined through the new parameter β , as follows:

$$\alpha = 3\beta\gamma, \quad (2.5)$$

$$M = \beta \left(1 - \frac{3\beta\gamma}{2} \right). \quad (2.6)$$

When $\gamma = 0$, $M = \beta$ and the Mannheim-Kazanas black hole coincides with the Schwarzschild-de Sitter solution in General Relativity.

The γr term is particularly significant in explaining the flat rotation curves of galaxies. In standard GR, flat rotation curves require additional mass (dark matter) at large distances from the galactic center. In conformal gravity, the γr term provides a natural explanation for the observed rotation curves without requiring dark matter.

The $-kr^2$ term is associated with a cosmological contribution and is negligible on galactic scales. It becomes relevant at even larger scales, possibly connecting to cosmological acceleration. The Mannheim-Kazanas solution has been used to fit galactic rotation curves with

only ordinary (baryonic) matter. Although the solution can fit many galactic rotation curves, its universal applicability to all galaxies and consistency with other gravitational phenomena (e.g., lensing, galaxy clusters) requires further scrutiny.

Various properties and generalizations of the Mannheim-Kazanas black holes, with an emphasis on particle motion, gravitational lensing, and Hawking radiation, have been studied in [14, 20–27].

3 Jizba-Mudruňka solution

Recently, another class of spherically symmetric solutions in the Weyl gravity was obtained using Newman-Penrose formalism [2]. The metric function of these solutions has the form:

$$f(r) = R^2(r) \left(\frac{1 - \alpha + kr_0^2}{\rho^2(r)} - \frac{6M + 2\gamma r_0^2}{3\rho^3(r)} + \frac{\gamma}{\rho(r)} - k \right), \quad R(r) = \sqrt{r^2 + r_0^2}, \quad (3.1)$$

where one fixes

$$\frac{1}{\rho(r)} = \int_r^\infty \frac{dr}{R^2(r)} = \frac{1}{r_0} \left(\frac{\pi}{2} - \arctan \frac{r}{r_0} \right), \quad (3.2)$$

so that, for $r \gg r_0$, we have

$$\frac{\rho(r)}{r} = 1 + \mathcal{O} \left(\frac{r_0}{r} \right)^2.$$

Therefore, asymptotically,

$$f(r) = 1 - \alpha - \frac{2M}{r} + \gamma r - kr^2 + \mathcal{O} \left(\frac{r_0}{r} \right)^2, \quad (3.3)$$

and we obtain the Mannheim-Kazanas solution as $r_0 \rightarrow 0$.

On the other hand, we have

$$\lim_{r \rightarrow -\infty} \rho(r) = \frac{r_0}{\pi}, \quad (3.4)$$

and

$$\lim_{r \rightarrow -\infty} \frac{f(r)}{r^2} = \pi^2 \frac{1 - \alpha}{r_0^2} - \frac{\pi\gamma}{r_0} \left(\frac{2\pi^2}{3} - 1 \right) - \frac{2M\pi^3}{r_0^3} + k(\pi^2 - 1). \quad (3.5)$$

The electric charge of the Maxwell field Q , $\mathcal{A}_a dx^a = \frac{Q}{R(r)} dt$, satisfies [2]

$$1 - (1 - \alpha + kr_0^2)^2 - 6M\gamma - 2\gamma^2 r_0^2 = \frac{3G_W^2 Q^2}{2}. \quad (3.6)$$

Therefore, if we consider the uncharged solution, for consistency with eq. (2.4), we will define M and α through the parameter β ,

$$\begin{aligned} \alpha &= 3\beta\gamma + kr_0^2, \\ M &= \beta \left(1 - \frac{3\beta\gamma}{2} \right) - \frac{\gamma r_0^2}{3}. \end{aligned} \quad (3.7)$$

Then, in the limit $r_0 \rightarrow 0$, relations (2.5) and (2.6) are reproduced.

The parameter r_0 is the minimum value of $R(r)$, which corresponds to $r = 0$. Requiring that the metric function $f(r)$ must be positive for a wormhole solution at $r = 0$, we see that for M/r_0 smaller than,

$$\frac{M}{r_0} < \frac{1 - \alpha}{\pi} - \gamma r_0 \left(\frac{1}{3} - \frac{2}{\pi^2} \right) + k r_0^2 \frac{\pi^2 - 4}{\pi^3}, \quad (3.8)$$

$r = 0$ is the position of the wormhole throat.

At $r \rightarrow -\infty$ the asymptotic of the wormholes obeying the above inequality (3.8) may be either de Sitter or anti-de Sitter one, depending on the sign of $f(r)/r^2$ in this limit. If, in addition to eq. (3.8), we have

$$\frac{M}{r_0} > \frac{1 - \alpha}{2\pi} - \gamma r_0 \left(\frac{1}{3} - \frac{1}{2\pi^2} \right) + k r_0^2 \frac{\pi^2 - 1}{2\pi^3}, \quad (3.9)$$

then, the wormhole's throat is a passage to the de Sitter universe. When, otherwise,

$$\frac{M}{r_0} < \frac{1 - \alpha}{2\pi} - \gamma r_0 \left(\frac{1}{3} - \frac{1}{2\pi^2} \right) + k r_0^2 \frac{\pi^2 - 1}{2\pi^3}, \quad (3.10)$$

the asymptotic values of $f(r)/r^2$ is larger than zero, and we have the anti-de Sitter (AdS) asymptotic.

A symmetric wormhole is possible only with two AdS asymptotics on both sides of the throat for a specific relation between the constants M and γ ,

$$M = -\frac{\gamma r_0^2}{3}. \quad (3.11)$$

Indeed, then the second term in the metric function (3.1) vanishes, which is the necessary, but not sufficient, condition for the symmetry of the metric relatively the throat.

For the neutral case, there is a symmetric wormhole with a negative asymptotic mass, which was considered in [2], provided

$$\gamma = \frac{2}{3\beta} = \frac{\pi}{r_0} \implies M = -\frac{\pi}{3} r_0 < 0,$$

then eq. (3.11) is satisfied and

$$f(r) = \frac{r^2 + r_0^2}{L^2} + \frac{r^2 + r_0^2}{r_0^2} \left(\frac{\pi^2}{4} - \arctan^2 \frac{r}{r_0} \right) \quad (3.12)$$

$$\left(k \equiv -\frac{1}{L^2}, \quad \alpha = 2 - k r_0^2 = 2 + \frac{r_0^2}{L^2} \right).$$

There is also a symmetric wormhole solution with positive mass for

$$\beta = 0, \quad M = -\frac{\gamma r_0^2}{3} = \frac{\pi r_0}{3} > 0.$$

In this case, we have

$$f(r) = \frac{r^2 + r_0^2}{L^2} - \frac{r^2 + r_0^2}{r_0^2} \left(\frac{\pi^2}{4} - \arctan^2 \frac{r}{r_0} \right) \quad (3.13)$$

$$\left(k \equiv -\frac{1}{L^2}, \quad \alpha = -k r_0^2 = \frac{r_0^2}{L^2} \right).$$

Here we have a wormhole only when

$$r_0 > \frac{\pi L}{2}.$$

For smaller values of r_0 , the throat is hidden by the event horizons, located at $r = \pm r_h$, where

$$r_h = r_0 \tan \sqrt{\frac{\pi^2}{4} - \frac{r_0^2}{L^2}},$$

and we obtain two asymptotically AdS black holes. It is interesting to note that for $r_0 \ll L$, we have

$$r_h = \frac{L^2}{r_0} + \mathcal{O}(r_0),$$

so that the horizons approach the AdS bounds, when decreasing r_0 .

In the present work, we focus on perturbations around asymptotically flat or de Sitter black holes and wormholes, leaving the more exotic anti-de Sitter case for future investigation.

4 Wavelike equations and effective potentials

Gravitational perturbations governed by a fourth-order differential equation present a highly challenging problem, raising several fundamental questions about the nature of such perturbations' propagation. Therefore, as a first step toward a comprehensive analysis of spacetime perturbations, we will focus on perturbations of test scalar, electromagnetic, and neutrino fields. In many cases, the evolution of gravitational field perturbations is qualitatively similar to that of matter fields. Indeed, in the high-frequency regime ($\ell \rightarrow \infty$), quasinormal modes typically do not depend on the spin of the field. However, exceptions have been observed, as described in [28], and are often associated with higher-order curvature terms [29, 30] or cosmological factors [31]. Therefore, we cannot rule out the possibility that gravitational perturbations introduce unique features into the quasinormal spectrum.

The scalar (Φ), electromagnetic (A_μ), and Dirac (Ψ_{Dirac}) fields in a curved spacetime obey the general covariant equations:

$$\frac{1}{\sqrt{-g}} \partial_\mu (\sqrt{-g} g^{\mu\nu} \partial_\nu \Phi) = 0, \quad (4.1a)$$

$$\frac{1}{\sqrt{-g}} \partial_\mu (F_{\rho\sigma} g^{\rho\nu} g^{\sigma\mu} \sqrt{-g}) = 0, \quad (4.1b)$$

$$\gamma^\alpha \left(\frac{\partial}{\partial x^\alpha} - \Gamma_\alpha \right) \Psi_{Dirac} = 0, \quad (4.1c)$$

where $F_{\mu\nu} = \partial_\mu A_\nu - \partial_\nu A_\mu$ is the electromagnetic tensor, γ^α are (noncommutative) gamma matrices and Γ_α are spin connections. After separation of variables and implying static, spherically symmetric background, these equations (4.1) can be reduced to the wavelike form with an effective potential [7, 8, 32]:

$$\frac{d^2 \Psi}{dr_*^2} + (\omega^2 - V(r)) \Psi = 0, \quad (4.2)$$

where the ‘‘tortoise coordinate’’ r_* is defined as follows

$$dr_* \equiv \frac{dr}{f(r)}. \quad (4.3)$$

From (3.1) it follows that the expression

$$\frac{f(r)}{R^2(r)} = P(\rho(r)) \quad (4.4)$$

depends on $\rho(r)$ only. Here we have introduced the function

$$P(\rho) \equiv \frac{1 - \alpha + kr_0^2}{\rho^2} - \frac{6M + 2\gamma r_0^2}{3\rho^3} + \frac{\gamma}{\rho} - k = \frac{1 - 3\beta\gamma}{\rho^2} - \frac{2\beta - 3\beta^2\gamma}{\rho^3} + \frac{\gamma}{\rho} - k, \quad (4.5)$$

which does not depend on r_0 once α and M are given in terms of the parameter β through (3.7).

Therefore, the tortoise coordinate is also a function of ρ ,

$$dr_* = \frac{dr}{f(r)} = \frac{dr}{R^2(r)P(\rho(r))} = \frac{d\rho}{\rho^2 P(\rho)}. \quad (4.6)$$

The effective potentials for scalar ($s = 0$) and electromagnetic ($s = 1$) fields can be written in the following form,

$$V(r) = f(r) \frac{\ell(\ell + 1)}{R(r)^2} + \frac{1 - s}{R(r)} \cdot \frac{d^2 R}{dr_*^2} = \ell(\ell + 1)P(\rho(r)) + \frac{1 - s}{R(r)} \cdot \frac{d^2 R}{dr_*^2}, \quad (4.7)$$

where $\ell = s, s + 1, s + 2, \dots$ is the multipole number appearing as a result of separation of angular variables, and $s = 0$ ($s = 1$) for the scalar (electromagnetic) field respectively.

It is interesting to note that the effective potential for $s = 1$ is proportional to $P(\rho)$, and, since the tortoise coordinate is also defined in (4.6) through $P(\rho)$, the wavelike equation (4.2) does not depend on r_0 when we express M in terms of the parameter β .

For the Dirac field we have two isospectral potentials, corresponding to the two degrees of freedom (chiralities),

$$V_{\pm}(r) = W^2 \pm \frac{dW}{dr_*}, \quad W \equiv \left(\ell + \frac{1}{2}\right) \frac{\sqrt{f(r)}}{R(r)} = \left(\ell + \frac{1}{2}\right) \sqrt{P(\rho(r))}. \quad (4.8)$$

The corresponding isospectral solutions of the Dirac equation are linked by the Darboux transformation,

$$\Psi_+ \propto \left(W + \frac{d}{dr_*}\right) \Psi_-. \quad (4.9)$$

Consequently, from the point of view of quasinormal mode calculations, it is sufficient to use only one of the effective potentials. We use here $V_+(r)$, because the WKB method is usually more accurate for such choice. Since both potentials are again defined through $P(\rho)$ and its derivatives with respect to the tortoise coordinate, we conclude that the perturbation equation for the test Dirac field does not depend on r_0 when we parametrize M via the parameter β .

Thus, only the minimally coupled test scalar field depends on the wormhole's throat size r_0 in the chosen parametrization of the metric. Figures 2 and 3 show that, for certain parameter values, the effective potential for the scalar field can exhibit a negative gap. This indicates that the stability of the perturbations is not guaranteed, necessitating time-domain integration of the wave equations to observe the behavior up to the stage of asymptotic tails.

It is important to note that, although the perturbation equations for the Maxwell and Dirac fields in terms of the parameter β do not depend on r_0 , being essentially the same

for the Mannheim-Kazanas black holes and Jizba-Mudruška black holes and wormholes, the asymptotic mass depends on the value of the throat size r_0 , unless $\gamma = 0$. If the dark matter term $\gamma \neq 0$, the quasinormal modes measured in units of the asymptotic mass, ωM , depend on the value of r_0 . Namely, both the oscillation frequency and the damping rate increase with r_0 when $\gamma < 0$ and decrease for $\gamma > 0$:

$$\omega M = \omega \beta \left(1 - \frac{3\beta\gamma}{2} - \frac{\gamma r_0^2}{3\beta} \right).$$

5 Exact solutions in the limit of vanishing black-hole mass

Here we will consider a few cases of vacuum spacetimes allowing for exact analytic solutions. We will be limited by those values of the parameters γ which provide asymptotically de Sitter-like solution with a cosmological event horizon in the far zone, rather than anti-de Sitter like asymptotic. Therefore, for example, when the cosmological constant vanishes ($k = 0$), we are limited by negative values of γ .

5.1 Zero cosmological constant, $\gamma < 0$

In the limit of vanishing effective cosmological constant $k = 0$ and black-hole mass $M = 0$ ($\beta = 0, \alpha = 0$) for $\gamma < 0$, the Mannheim-Kazanas (2.4) metric function takes the simple form:

$$f(r) = 1 - \frac{r}{r_c}, \quad (5.1)$$

where $r_c = -1/\gamma$ is the cosmological horizon.

The derivative of the metric function (5.1) is a constant, and the perturbation equations are greatly simplified

$$\left(1 - \frac{r}{r_c} \right) \left(\left(1 - \frac{r}{r_c} \right) \Psi''(r) - \frac{1}{r_c} \Psi'(r) \right) + \left(w^2 - \left(1 - \frac{r}{r_c} \right) \frac{\ell(\ell+1) - (1-s)r/r_c}{r^2} \right) \Psi(r) = 0 \quad (5.2)$$

and its general solution for the electromagnetic perturbations ($s = 1$) is

$$\Psi(r) = \left(1 - \frac{r}{r_c} \right)^{-i\omega r_c} \left(C_1 \cdot r^{-\ell} {}_2F_1(-\ell, -\ell - 2i\omega r_c, -2\ell \mid r/r_c) + C_2 \cdot r^{\ell+1} {}_2F_1(\ell+1, \ell+1 - 2i\omega r_c, 2\ell+2 \mid r/r_c) \right), \quad (5.3)$$

where ${}_2F_1(a, b, c \mid z)$ is the hypergeometric function, which is regular at $r = 0$. Therefore, for the regular solutions we take $C_1 = 0$.

Since $\ell + 1 > 0$ the quasinormal boundary conditions at $r \rightarrow r_c - 0$ (purely outgoing wave) are satisfied iff $\ell + 1 - 2i\omega r_c = -n$, where n is nonnegative integer. Thus, we obtain the quasinormal spectrum,

$$\omega_n = -i \frac{\ell + 1 + n}{2r_c}, \quad n = 0, 1, 2, \dots \quad (5.4)$$

For the scalar field ($s = 0$), the general solution can be represented in a similar form,

$$\Psi(r) = \left(1 - \frac{r}{r_c}\right)^{-i\omega r_c} \left(C_1 \cdot r^{-\ell} {}_2F_1 \left(-\ell + \frac{1}{2i\Omega r_c}, -\ell - 2i\Omega r_c, -2\ell \mid r/r_c \right) + C_2 \cdot r^{\ell+1} {}_2F_1 \left(\ell + 1 + \frac{1}{2i\Omega r_c}, \ell + 1 - 2i\Omega r_c, 2\ell + 2 \mid r/r_c \right) \right), \quad (5.5)$$

where

$$\Omega = \omega \frac{1 + \sqrt{1 - \omega^{-2} r_c^{-2}}}{2},$$

and the quasinormal modes can be given by the following expression:

$$\omega_n = -\frac{i}{2r_c} \left(\ell + 1 + n - \frac{1}{\ell + 1 + n} \right), \quad n = 0, 1, 2, \dots \quad (5.6)$$

One should note that, for $\ell = n = 0$, formula (5.6) gives the eigenvalue $\omega = 0$, for which $\Omega = -i/2r_c$. The corresponding algebraically special solution $\Psi(r) = C_2 \cdot r$ is not dynamic, being a constant contribution to the scalar field in (4.1a), $\Phi \propto \Psi/r$, which redefines the vacuum state of the scalar field.

Once we exclude $\ell = n = 0$ from the quasinormal spectrum, the fundamental mode of the $\ell = 0$ spectrum corresponds to $n = 1$ in (5.6) and we can rewrite the expression (5.6) for $\ell = 0$ as follows

$$\omega_{n,\ell=0} = -\frac{i}{2r_c} \left(2 + n - \frac{1}{2 + n} \right), \quad n = 0, 1, 2, \dots \quad (5.7)$$

which evidently coincides with expression (5.6) for $\ell = 1$. Therefore, quasinormal modes of the test scalar field for $\ell = 0$ and $\ell = 1$ coincide in the limit of vanishing black-hole mass.

5.2 Nonzero cosmological constant

When k is nonzero, we define

$$\gamma = -\frac{1}{r_c} + kr_c, \quad (5.8)$$

and assume that $k > -r_c^{-2}$, so that r_c is again the cosmological horizon,

$$f(r) = \left(1 - \frac{r}{r_c}\right) (1 + kr_c \cdot r). \quad (5.9)$$

It is interesting to note that after introducing the new variable

$$\tilde{r} = r \cdot \frac{1 + kr_c^2}{1 + kr_c \cdot r}, \quad 0 \leq \tilde{r} \leq r_c, \quad (5.10)$$

the wavelike equation for $s = 1$ takes the form of (5.2) with the effective frequency

$$\tilde{\omega} = \frac{\omega}{1 + kr_c^2}. \quad (5.11)$$

Therefore, we conclude that, for the electromagnetic perturbations,

$$\omega_n = (1 + kr_c^2) \tilde{\omega} = -i \frac{1 + kr_c^2}{2r_c} (\ell + 1 + n). \quad (5.12)$$

When $k = r_c^{-2}$ then $\gamma = 0$, and (5.12) is reduced to the de Sitter spectrum [33, 34]:

$$\omega_n = -i \frac{\ell + 1 + n}{r_c} \quad (s = 1). \quad (5.13)$$

For $s = 0$ the equation has an additional singular point and the solution cannot be expressed in terms of the hypergeometric function. Analysis of the corresponding Heun equation is beyond the scope of the present paper.

In sec. 8, we will show that for those cases when we were able to find the exact analytic solutions of the vacuum spacetime, quasinormal modes of black holes tend to those of the vacuum when mass of the black hole goes to zero. This could be expected by analogy with [35] where it was found that for general spherically symmetric and asymptotically de Sitter black holes in metric theories of gravity we have

$$\omega_n = \omega_n^{(dS)} \left(1 - \frac{r_0(1 + \epsilon)}{2r_c} + \mathcal{O}\left(\frac{r_e}{r_c}\right)^2 \right) = \omega_n^{(dS)} \left(1 - \frac{M}{r_c} + \mathcal{O}\left(\frac{M}{r_c}\right)^2 \right), \quad (5.14)$$

where ϵ is deviation of the event horizon radius from its Schwarzschild limit. This relation is valid when the dark matter term vanishes, but when $\gamma \neq 0$, the correction terms containing the black hole mass must be different.

6 Shadows

Shadows cast by black holes in the presence of dark matter have been extensively studied in numerous publications, making it difficult to review the entire body of work within the scope of this paper. Here, we highlight a selection of studies that employ various approaches to modeling dark matter [36–46], as well as several works that develop general formalisms for determining the parameters of black hole and wormhole shadows [47–50].

The literature on wormhole shadows is similarly extensive (see, for example, [51–55] and references therein). A comprehensive analysis of various wormhole configurations, as presented in [49], could also prove valuable for further research.

We consider the motion in the equatorial plane ($\theta = \pi/2$, $d\theta = 0$) along the null geodesic,

$$ds^2 = -f(r)dt^2 + \frac{dr^2}{f(r)} + R(r)^2 d\phi^2 = 0, \quad (6.1)$$

$$\frac{d^2r}{dt^2} = -\frac{f(r)f'(r)}{2} dt^2 + \frac{f'(r)}{2f(r)} dr^2 + f(r)R(r)R'(r) d\phi^2. \quad (6.2)$$

The circular orbit $r = r_c$, $dr = 0$, $d^2r = 0$, satisfies

$$f'(r_c) = 2f(r_c) \frac{R'(r_c)}{R(r_c)}, \quad (6.3)$$

and the corresponding angular frequency,

$$\Omega_c = \frac{d\phi}{dt} = \frac{\sqrt{f(r_c)}}{R(r_c)}. \quad (6.4)$$

We note that (6.3) is the extremum condition of the righthand side of (6.4), therefore,

$$\Omega_c = \max_r \frac{\sqrt{f(r)}}{R(r)} = \max_\rho \sqrt{P(\rho)}, \quad (6.5)$$

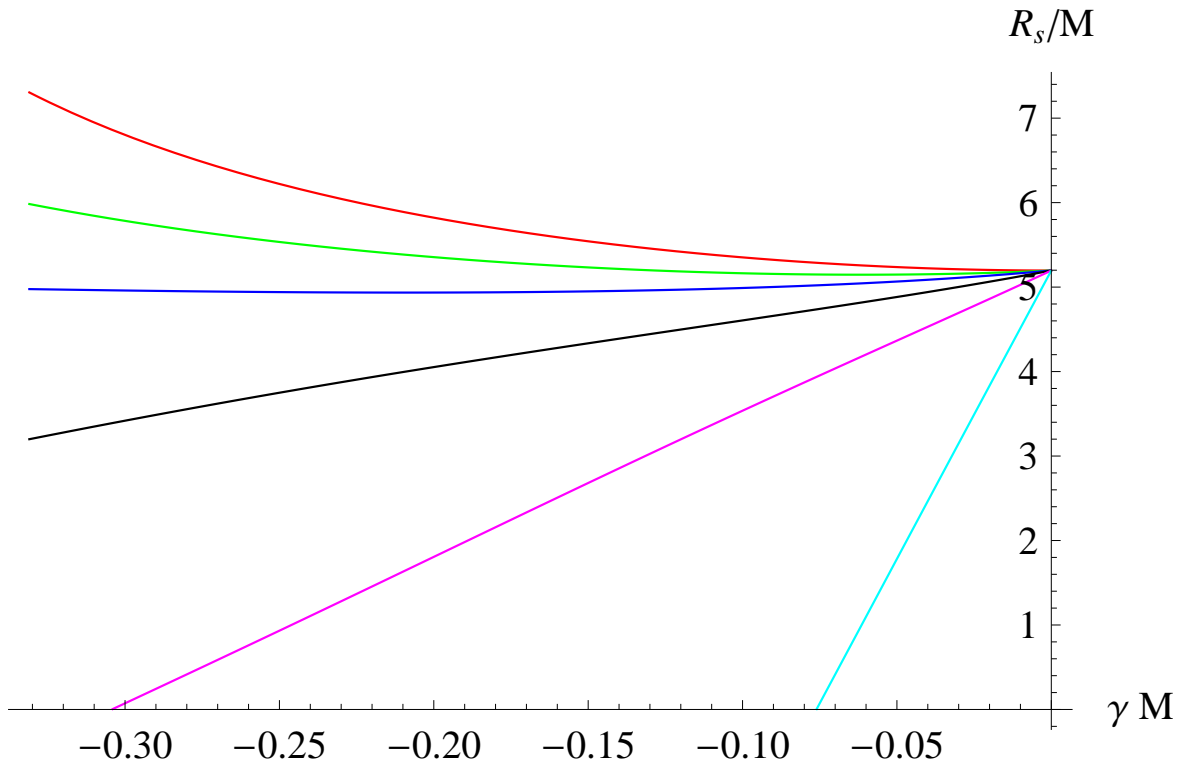


Figure 1. Radius of the shadow cast by a black hole or wormhole as a function of γ for various values of r_0 : $r_0 = 0$ (red, top), $r_0 = M$ (green), $r_0 = 1.5M$ (blue), $r_0 = 2M$ (black), $r_0 = 3.14M$ (pink), $6.28M$ (bottom, cyan); $k = 0$.

where the function $P(\rho)$ given by (4.5) in terms of the parameter β does not depend on r_0

$$P(\rho) = \frac{1 - 3\beta\gamma}{\rho^2} - \frac{2\beta - 3\beta^2\gamma}{\rho^3} + \frac{\gamma}{\rho} - k. \quad (6.6)$$

The maximum of the function $P(\rho)$ is reached at $\rho = 3\beta$. Finally, we find

$$\Omega_c = \sqrt{P(3\beta)} = \sqrt{\frac{1 + 3\beta\gamma}{27\beta^2} - k}. \quad (6.7)$$

The shadow radius visible by a remote observer,

$$R_s \equiv \frac{1}{\Omega_c} = \frac{1}{\sqrt{P(3\beta)}} = \frac{3\sqrt{3}\beta}{\sqrt{1 + 3\beta\gamma - 27k\beta^2}}. \quad (6.8)$$

When $\gamma = k = 0$ ($\beta = M$) we reproduce the well known formula for the radius of the shadow of the Schwarzschild black hole. In fig. 1 the radius of the shadow is shown in units of the asymptotic black hole/wormhole mass M . There we can see that once r_0 is small, the radius of the shadow grows once the absolute value of γ is increased. However, at some r_0 the situation changes to the opposite: larger absolute values of γ lead to smaller radius of the shadow, so that for the near extreme wormholes with $r_0 = 6.28M$, the radius of the shadow goes to zero at some critical values of γ corresponding to the limit $\beta \rightarrow 0$.

By substituting $r = r_c + \delta r$ into (6.1), we obtain the equation for the radial coordinate of the photons that are leaving the circular orbit,

$$\left(\frac{d}{dt}\delta r\right)^2 = \lambda^2 \delta r^2 + \mathcal{O}(\delta r)^3, \quad (6.9)$$

where λ is the Lyapunov exponent, satisfying,

$$\lambda^2 = -\frac{1}{2P(\rho(r))} \frac{d^2 P}{dr_*^2} \Bigg|_{r=r_c} = -\frac{\rho^4 P(\rho) P''(\rho)}{2} \Bigg|_{\rho=3\beta} = \frac{1 + 3\beta\gamma}{27\beta^2} - k. \quad (6.10)$$

7 Numerical methods for the calculation of quasinormal modes

The quasinormal modes of asymptotically flat black holes are the eigenvalues of the wavelike equation (4.2) with the boundary conditions:

$$\Psi(r_* \rightarrow \pm\infty) \propto e^{\pm i\omega r_*}, \quad (7.1)$$

which correspond to a purely ingoing wave at the event horizon ($r_* \rightarrow -\infty$) and a purely outgoing wave at spatial infinity ($r_* \rightarrow \infty$). When the spacetime is asymptotically de Sitter one, the outgoing boundary condition is imposed on the de Sitter horizon instead.

The same boundary conditions are appropriate to traversable wormholes, where for asymptotically flat spacetimes, $r_* \rightarrow -\infty$ corresponds to spatial infinity in the other universe [9]. If a wormhole is asymptotically de Sitter at one or both asymptotics, then, again, we imply purely outgoing boundary conditions at the de Sitter horizon. The similarity in boundary conditions for black holes and wormholes allows one to use the same techniques for finding quasinormal of both compact objects.

In this work, we deal only with the decaying modes, characterized by $Im(\omega) < 0$, and restrict our analysis to real oscillation frequencies with $Re(\omega) > 0$. We provide a brief overview of the WKB approximation, time-domain integration, and the Bernstein polynomial methods, which are employed to compute the quasinormal frequencies of black holes and wormholes.

7.1 WKB approach

The WKB method is one of the most widely used techniques for calculating low-lying quasinormal modes, owing to its speed, automation, and generally sufficient accuracy in most cases (see [56–65] for recent examples of applications). This method is based on matching the asymptotic solutions, which satisfy the quasinormal boundary conditions (7.1), with the Taylor expansion of the potential around its peak, through the two turning points defined by the equation

$$V(r_*) = \omega^2.$$

As a result, the WKB method is particularly effective when the effective potential has a barrier shape with a single peak. Even in cases where a small negative gap exists near the event horizon, as illustrated in Figures 2 and 3, the WKB approach can still provide a reliable approximation for the dominant quasinormal frequencies.

The first-order WKB formula corresponds to the eikonal approximation, which becomes exact in the limit $\ell \rightarrow \infty$. The general WKB expression for quasinormal frequencies can be represented as an expansion around the eikonal limit [66]:

$$\begin{aligned} \omega^2 = & V_0 + A_2(\mathcal{K}^2) + A_4(\mathcal{K}^2) + A_6(\mathcal{K}^2) + \dots \\ & - i\mathcal{K}\sqrt{-2V_2} (1 + A_3(\mathcal{K}^2) + A_5(\mathcal{K}^2) + A_7(\mathcal{K}^2) + \dots), \end{aligned} \quad (7.2)$$

where the matching conditions for the quasinormal modes impose

$$\mathcal{K} = n + \frac{1}{2}, \quad n = 0, 1, 2, \dots,$$

with n being the overtone number. Here, V_0 is the value of the effective potential at its maximum, V_2 is the second derivative of the potential at this point, and A_i for $i = 2, 3, 4, \dots$ are the i -th order WKB correction terms beyond the eikonal approximation. These corrections depend on \mathcal{K} and the derivatives of the potential at its maximum up to the order $2i$. Explicit forms for the corrections A_i can be found in [67] for the second and third WKB orders, in [68] for the 4th-6th orders, and in [69] for the 7th-13th orders. If the differences between the results obtained at consecutive WKB orders, such as the 5th, 6th, and 7th, are relatively small, it indicates that the WKB method is stable. In such cases, the relative error is typically of the same magnitude as these differences or smaller. Here we present the data obtained mostly by the 10th WKB order with Padé approximants [69], where the WKB series demonstrates a kind of plateau of “relative convergence”.

7.2 Time-domain integration

The Gundlach-Price-Pullin time-domain integration scheme [70] is a widely used numerical method for analyzing the evolution of perturbations in black-hole spacetimes and extracting quasinormal modes. This approach is based on solving the wave equation, typically written in the form:

$$\frac{\partial^2 \Psi}{\partial t^2} - \frac{\partial^2 \Psi}{\partial r_*^2} + V(r_*)\Psi = 0,$$

where Ψ is the perturbation field, r_* is the tortoise coordinate, and $V(r_*)$ is the effective potential. The method discretizes this wave equation on a numerical grid in characteristic coordinates $u = t - r_*$ and $v = t + r_*$, transforming the equation into a form suitable for finite difference integration:

$$\Psi(N) = \Psi(W) + \Psi(E) - \Psi(S) - \Delta^2 V(S) \frac{\Psi(W) + \Psi(E)}{8} + \mathcal{O}(\Delta^4), \quad (7.3)$$

Here, $N \equiv (u + \Delta, v + \Delta)$, $W \equiv (u + \Delta, v)$, $E \equiv (u, v + \Delta)$, and $S \equiv (u, v)$ represent neighboring points on the computational grid. This formulation avoids coordinate singularities near the event horizon, ensuring numerical stability and allowing for the accurate evolution of perturbations over time. This scheme captures the full time-domain evolution, including the initial burst, the quasinormal ringing phase, and the late-time tails.

Once the time-domain profiles of the perturbations are obtained, the Prony method is employed to extract the quasinormal frequencies. The method fits the time-domain signal $\Psi(t)$ to a sum of exponentially damped sinusoids:

$$\Psi(t) = \sum_{i=1}^N A_i e^{-i\omega_i t},$$

where ω_i represents the complex frequency. By solving the least squares problem for the coefficients A_i and frequencies ω_i , the contribution of the dominant modes can be isolated and analyzed. The combination of the Gundlach-Price-Pullin integration scheme and the Prony method provides a robust approach for determining quasinormal frequencies, offering insights into the stability and dynamics of perturbations in various space-time geometries.

7.3 Bernstein polynomial method

The Bernstein polynomial method offers a numerical approach to approximate the solutions of differential equations by expanding the unknown function in terms of Bernstein polynomials. This method is particularly useful for handling boundary value problems due to the properties of Bernstein polynomials in approximating continuous functions over finite intervals.

Following [71], we introduce the compact coordinate,

$$u \equiv \frac{\frac{1}{r} - \frac{1}{r_c}}{\frac{1}{r_h} - \frac{1}{r_c}}, \quad (7.4)$$

where r_h is the event horizon of the black hole and r_c is the cosmological horizon. For the asymptotically flat spacetime $r_c \rightarrow \infty$. For the traversable wormhole r_h corresponds to the de Sitter horizon in the universe beyond the throat. So that for all the object under consideration $0 \leq u \leq 1$.

We introduce the function $\psi(u)$, which is regular at $u = 0$ and $u = 1$ when ω is a quasinormal mode,

$$\Psi(u) = F(u, \omega)\psi(u), \quad (7.5)$$

where the prefactor $F(u, \omega)$ is defined from the characteristic equations at the singular points of the wavelike equation (4.2).

We approximate the solution $\psi(u)$ using Bernstein polynomials over the interval $[0, 1]$:

$$\psi(u) \approx \sum_{k=0}^N c_k B_{k,N}(u), \quad (7.6)$$

where c_k are coefficients to be determined, N is the degree of the polynomial, and $B_{k,N}(u)$ are the Bernstein basis polynomials defined as:

$$B_{k,N}(u) = \frac{N!}{k!(N-k)!} u^k (1-u)^{N-k}. \quad (7.7)$$

Then we substitute the Bernstein expansion into the perturbation equation and use a Chebyshev collocation grid of $N + 1$ points,

$$u_p = \frac{1}{2} \left(1 - \cos \frac{p \cdot \pi}{N} \right) = \sin^2 \frac{p \cdot \pi}{2N}, \quad p = \overline{0, N}.$$

Thus, the problem is reduced to a set of linear equations with respect to c_k , which has nontrivial solutions iff the corresponding coefficient matrix is singular. The elements of the coefficient matrix are polynomials of ω , therefore, we solve numerically the eigenvalue problem for a matrix pencil with respect to the quasinormal frequencies ω , which is a linear problem.

In order to exclude the spurious eigenvalues, which appear due to finiteness of the polynomial basis in (7.6), we compare both the eigenfrequencies and corresponding approximating polynomials for different values of N , as proposed in [72]. Namely, from each set of the solutions we take the eigenvalues that differ less than the required accuracy and, for each pair of the corresponding eigenfunction, $\psi^{(1)}$ and $\psi^{(2)}$, we calculate

$$1 - \frac{|\langle \psi^{(1)} | \psi^{(2)} \rangle|^2}{\|\psi^{(1)}\|^2 \|\psi^{(2)}\|^2} = \sin^2 \alpha,$$

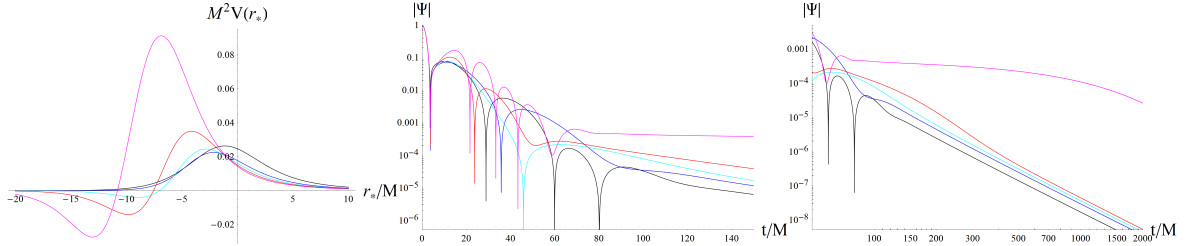


Figure 2. The effective potentials (left panel) and time-domain profiles (semi-log plot for the ring-down and log-log plot for the late-time tails) for the scalar perturbations ($\ell = 0$) of the asymptotically flat Jizba-Mudruňka solution ($k = 0$, $\gamma = 0$, $\alpha = 0$, $M = \beta$): $r_0 = 0$ (black), $r_0 = 3M$ (blue), $r_0 = 4M$ (cyan), $r_0 = 5M$ (red), $r_0 = 6M$ (magenta). $r_0 = 0$ corresponds to the Schwarzschild black hole, for $0 < r_0 \leq \pi M$ there is a black hole, which differs from Schwarzschild, when $\pi M < r_0 < 2\pi M$ there is a throat, which connects the flat space to a de Sitter universe. The time-domain profile is calculated for $r = 3M$ ($r_* = 0$).

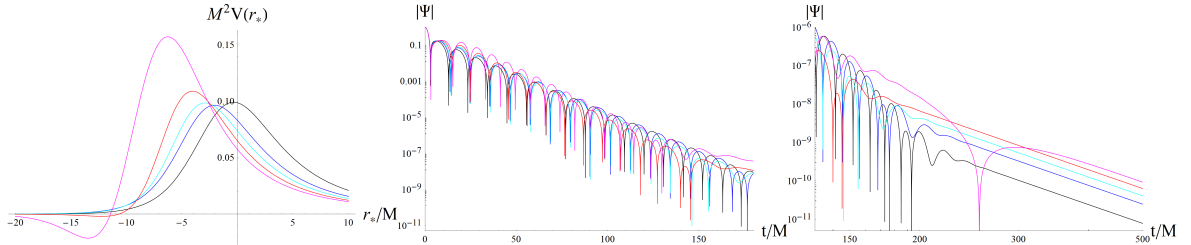


Figure 3. The effective potentials (left panel) and time-domain profiles (semi-log plot for the ring-down and log-log plot for the late-time tails) for the scalar perturbations ($\ell = 1$) of the asymptotically flat Jizba-Mudruňka solution ($k = 0$, $\gamma = 0$, $\alpha = 0$, $M = \beta$): $r_0 = 0$ (black), $r_0 = 3M$ (blue), $r_0 = 4M$ (cyan), $r_0 = 5M$ (red), $r_0 = 6M$ (magenta). $r_0 = 0$ corresponds to the Schwarzschild black hole, for $0 < r_0 \leq \pi M$ there is a black hole, which differs from Schwarzschild, when $\pi M < r_0 < 2\pi M$ there is a throat, which connects the flat space to a de Sitter universe. The time-domain profile is given for $r = 3M$ ($r_* = 0$).

where α is the angle between the vectors $\psi^{(1)}$ and $\psi^{(2)}$ in the L^2 -space. If all values of α are sufficiently small, we conclude that the obtained eigenvalues ω approximate the quasinormal frequencies, and better approximations correspond to larger N . We estimate the error by calculating the difference between the approximate eigenvalues of ω , corresponding to different values of N .

Bernstein polynomials possess excellent convergence properties for approximating continuous functions, which enhances the accuracy of the method. The method avoids issues related to divergent behaviors at the boundaries by working within a finite interval and using the appropriate boundary conditions. More details can be found in [71–73].

8 Quasinormal modes

The distinctive feature of the quasinormal spectrum of black holes and wormholes in the Weyl gravity is the presence of three branches of modes:

1. Schwarzschild branch of modes, which reduces to the well-known quasinormal modes of Schwarzschild spacetime when $\alpha = \gamma = k = 0$. In other words, these are modes

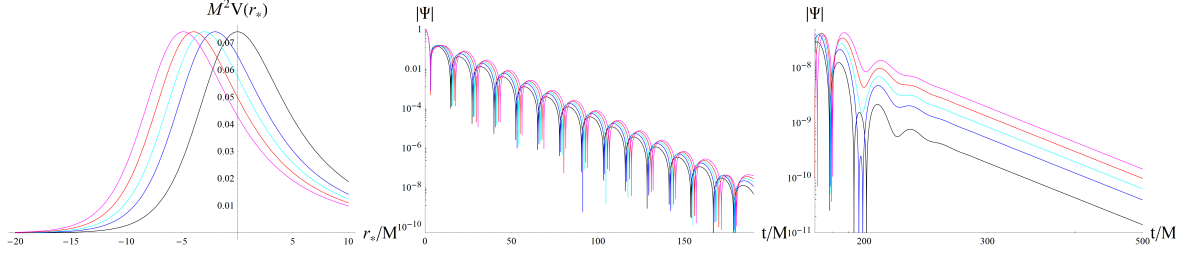


Figure 4. The effective potentials (left panel) and time-domain profiles (semi-log plot for the ring-down and log-log plot for the late-time tails) for the Maxwell perturbations ($\ell = 1$) of the asymptotically flat Jizba-Mudruňka solution ($k = 0$, $\gamma = 0$, $\alpha = 0$, $M = \beta$): $r_0 = 0$ (black), $r_0 = 3M$ (blue), $r_0 = 4M$ (cyan), $r_0 = 5M$ (red), $r_0 = 6M$ (magenta). $r_0 = 0$ corresponds to the Schwarzschild black hole, for $0 < r_0 \leq \pi M$ there is a black hole, which differs from Schwarzschild, when $\pi M < r_0 < 2\pi M$ there is a throat, which connects the flat space to a de Sitter universe. The time-domain profile is given for $r = 3M$ ($r_* = 0$).

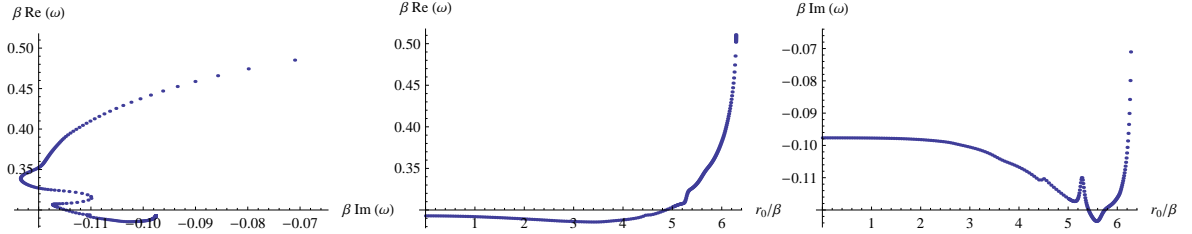


Figure 5. Scalar field perturbations ($\ell = 1$, $n = 0$) for $\gamma = 0$ and $k = 0$ ($M = \beta$, $\alpha = 0$), for various values of r_0 .

of Schwarzschild black holes corrected by the dark matter term γ and cosmological constant k .

2. Dark-matter-induced branch of quasinormal modes: When $k = 0$ and the mass of the black hole goes to zero, these modes tend to modes of empty spacetime in Weyl gravity, which are similar in nature to those in the de Sitter space.
3. de Sitter branch of frequencies: When $\gamma = 0$ and the mass vanishes, these modes go over into the modes of pure de Sitter spacetime [33, 34]. Thus, these modes are eigenvalues of empty de Sitter space corrected by the presence of a black hole.

All these branches are evident for the Mannheim-Kazanas solution [1], but not for the black holes and wormholes found in [2], as the limit $M \rightarrow 0$ is not well-defined for those solutions.

The Schwarzschild branch of modes is determined with remarkable accuracy using the WKB method, provided ℓ is not smaller than n . The longest-lived mode of this branch, corresponding to the fundamental mode of the Schwarzschild solution, is presented in Tables 1–3. However, the longest-lived modes of the other two branches can only be detected via time-domain integration, while the overtones require the application of the Bernstein polynomial method. From Fig. 6 we can see that the purely imaginary, i.e. non-oscillatory, quasinormal modes of the dark matter branch exist in the spectrum. When the analog of the de Sitter radius, determining the cosmological horizon owing to the dark matter term, is much larger

γ	$\omega (r_0 = 0)$	$\omega (r_0 = 3.14)$	$\omega (r_0 = 5.5)$	$\omega (r_0 = 6.28)$
0	0.292936-0.097660 i	0.285841-0.101134 i	0.332508-0.122606 i	0.501895-0.051487 i
-0.02	0.281714-0.095430 i	0.274984-0.098594 i	0.317741-0.117127 i	0.431138-0.094564 i
-0.04	0.270344-0.092994 i	0.263994-0.095850 i	0.301728-0.108877 i	0.391830-0.101732 i
-0.06	0.258802-0.090340 i	0.252844-0.092887 i	0.281835-0.105151 i	0.362062-0.100922 i
-0.08	0.247061-0.087457 i	0.241502-0.089689 i	0.266269-0.103320 i	0.333921-0.101787 i
-0.1	0.235089-0.084328 i	0.229939-0.086229 i	0.251729-0.099476 i	0.309310-0.099689 i
-0.12	0.222846-0.080937 i	0.218138-0.082479 i	0.237268-0.094096 i	0.286487-0.096700 i
-0.14	0.210284-0.077261 i	0.206090-0.078449 i	0.224242-0.088038 i	0.264066-0.093030 i
-0.16	0.197342-0.073273 i	0.193704-0.074176 i	0.210587-0.084766 i	0.241196-0.087394 i
-0.18	0.183940-0.068938 i	0.180844-0.069613 i	0.193964-0.080042 i	0.219571-0.080776 i
-0.2	0.169970-0.064212 i	0.167396-0.064688 i	0.177228-0.073654 i	0.198729-0.074040 i
-0.22	0.155281-0.059035 i	0.153215-0.059339 i	0.160483-0.066570 i	0.178081-0.068295 i
-0.24	0.139648-0.053323 i	0.138071-0.053489 i	0.143303-0.059122 i	0.156284-0.062179 i
-0.26	0.122703-0.046952 i	0.121583-0.047018 i	0.125028-0.051287 i	0.133666-0.054282 i
-0.28	0.103771-0.039695 i	0.103066-0.039704 i	0.104739-0.042483 i	0.110043-0.044799 i
-0.3	0.081407-0.031055 i	0.081056-0.031043 i	0.081794-0.032387 i	0.084300-0.033924 i
-0.32	0.051130-0.019409 i	0.051042-0.019402 i	0.051205-0.019688 i	0.051694-0.020230 i
-0.33	0.025484-0.009643 i	0.025473-0.009642 i	0.025495-0.009678 i	0.025552-0.009733 i
-0.331	0.021315-0.008063 i	0.021309-0.008062 i	0.021321-0.008083 i	0.021355-0.008116 i

Table 1. Fundamental quasinormal mode for $\ell = 1$ scalar field perturbations found by the 10th order WKB method with Padé approximants; $k = 0$, $\beta = 1$. The cases $r_0 = 0$ is the Mannheim-Kazanas BH, $r_0 = 3.14$ Jizba-Mudruška BH near the transition with the wormhole, $r_0 = 5.5$ Jizba-Mudruška wormhole, $r_0 = 6.28$ Jizba-Mudruška wormhole near the transition with the asymptotic AdS space.

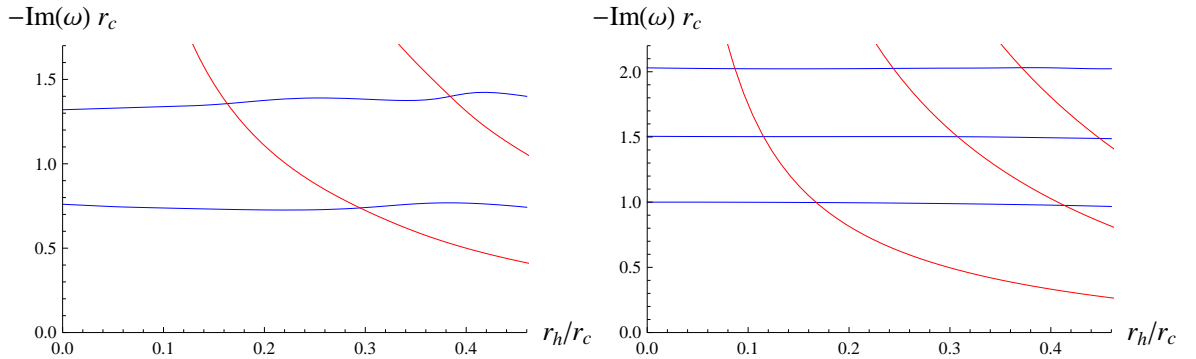


Figure 6. Imaginary part of the cosmological branch (blue) and black-hole branch (red) for the Mannheim-Kazanas solution ($r_0 = 0$) in the limit of vanishing effective cosmological constant ($k = 0$) for $s = \ell = 0$ (left panel) and $s = \ell = 1$ (right panel): As black-hole radius $r_h \rightarrow 0$ ($M \rightarrow 0$) the cosmological branch approaches the analytic solution, (5.4) and (5.6) for the electromagnetic and scalar perturbations respectively, while the black-hole branch ($\omega \propto r_h^{-1}$) diverges. The quasinormal frequencies were calculated using the Bernstein polynomial method.

than the black hole radius, these modes go over into the modes of empty spacetime in the Weyl gravity, given by Eqs. (5.4) and (5.6).

The modes associated with the Schwarzschild branch converge to a universal limit as the dark matter parameter γ approaches its extreme value. This limit is independent of both

γ	$\omega (\ell = 1)$	$\omega (\ell = 2)$	$\omega (\ell = 3)$
0	0.248263-0.092488 i	0.457596-0.095004 i	0.656899-0.095616 i
-0.02	0.240719-0.089675 i	0.443666-0.092112 i	0.636895-0.092704 i
-0.04	0.232964-0.086781 i	0.429305-0.089128 i	0.616255-0.089699 i
-0.06	0.224973-0.083795 i	0.414463-0.086044 i	0.594913-0.086591 i
-0.08	0.216711-0.080706 i	0.399085-0.082848 i	0.572786-0.083369 i
-0.1	0.208141-0.077502 i	0.383100-0.079525 i	0.549776-0.080018 i
-0.12	0.199213-0.074166 i	0.366424-0.076060 i	0.525765-0.076521 i
-0.14	0.189868-0.070678 i	0.348954-0.072431 i	0.500604-0.072858 i
-0.16	0.180029-0.067013 i	0.330555-0.068611 i	0.474105-0.069001 i
-0.18	0.169598-0.063136 i	0.311057-0.064566 i	0.446026-0.064915 i
-0.2	0.158440-0.059001 i	0.290229-0.060249 i	0.416039-0.060554 i
-0.22	0.146373-0.054543 i	0.267751-0.055592 i	0.383691-0.055851 i
-0.24	0.133127-0.049661 i	0.243155-0.050501 i	0.348319-0.050709 i
-0.26	0.118286-0.044196 i	0.215704-0.044820 i	0.308873-0.044976 i
-0.28	0.101128-0.037869 i	0.184112-0.038280 i	0.263522-0.038384 i
-0.3	0.080156-0.030103 i	0.145688-0.030317 i	0.208431-0.030372 i
-0.32	0.050828-0.019158 i	0.092232-0.019214 i	0.131890-0.019230 i
-0.33	0.025448-0.009611 i	0.046140-0.009619 i	0.065963-0.009620 i
-0.331	0.021294-0.008044 i	0.038605-0.008048 i	0.055190-0.008050 i

Table 2. Fundamental quasinormal mode for $\ell = 1, 2, 3$ electromagnetic field perturbations found by the 10th order WKB method with Padé approximants; $k = 0$, $\beta = 1$.

r_0 and the spin of the field under consideration, as illustrated in Tables 1–3. When mass of the black hole goes to zero these modes, being inverse proportional to it, diverges as shown in Fig. 6. When the dark matter term goes to zero these modes go over into the Schwarzschild ones.

We also observe that the spectrum of wormholes with large r_0 differs significantly from that of black holes, exhibiting much larger real oscillation frequencies, as shown in Tables 1–3. As demonstrated in Fig. 5, the transition between a black hole and a wormhole, which occurs at $r_0 = \pi\beta$, is not particularly remarkable. Quasinormal modes at the black hole–wormhole transition have been studied in several works [74, 75]. Typically, this transition is characterized by the onset of echoes once the wormhole is formed due to the appearance of a double peak in the effective potential. Here, however, no such doubling of the potential peak occurs during the transition to the wormhole state, and consequently, no echoes are observed.

The only notable feature of the black-hole-wormhole transition point is that the minimum of the real oscillation frequency occurs at $r_0 \approx 3\beta$ (see Fig. 5).

In the eikonal limit ($\ell \rightarrow \infty$), the effective potential does not depend on the spin,

$$V(r) = \left(\ell + \frac{1}{2}\right)^2 \left(P(\rho(r)) + \mathcal{O}\left(\frac{1}{\ell}\right)\right), \quad (8.1)$$

and its point of maximum is reached (cf. 6.7) for

$$\rho(r_m) = 3\beta + \mathcal{O}\left(\frac{1}{\ell}\right). \quad (8.2)$$

γ	$\omega (\ell = 1/2)$	$\omega (\ell = 3/2)$	$\omega (\ell = 5/2)$
0	0.182643-0.096566 i	0.380041-0.096408 i	0.574094-0.096305 i
-0.02	0.177102-0.093614 i	0.368476-0.093468 i	0.556614-0.093370 i
-0.04	0.171428-0.090546 i	0.356559-0.090427 i	0.538582-0.090337 i
-0.06	0.165598-0.087355 i	0.344250-0.087275 i	0.519939-0.087196 i
-0.08	0.159589-0.084030 i	0.331502-0.084003 i	0.500614-0.083937 i
-0.1	0.153373-0.080561 i	0.318256-0.080595 i	0.480521-0.080545 i
-0.12	0.146913-0.076935 i	0.304442-0.077037 i	0.459555-0.077004 i
-0.14	0.140166-0.073137 i	0.289974-0.073309 i	0.437587-0.073293 i
-0.16	0.133072-0.069147 i	0.274739-0.069385 i	0.414451-0.069386 i
-0.18	0.125557-0.064937 i	0.258594-0.065231 i	0.389935-0.065248 i
-0.2	0.117518-0.060470 i	0.241345-0.060804 i	0.363753-0.060834 i
-0.22	0.108811-0.055691 i	0.222723-0.056038 i	0.335505-0.056077 i
-0.24	0.099222-0.050513 i	0.202336-0.050840 i	0.304611-0.050883 i
-0.26	0.088420-0.044787 i	0.179567-0.045059 i	0.270152-0.045101 i
-0.28	0.075834-0.038240 i	0.153337-0.038430 i	0.230521-0.038463 i
-0.3	0.060303-0.030295 i	0.121398-0.030391 i	0.182359-0.030412 i
-0.32	0.038355-0.019210 i	0.076897-0.019233 i	0.115414-0.019240 i
-0.33	0.019226-0.009620 i	0.038479-0.009621 i	0.057728-0.009622 i
-0.331	0.016090-0.008050 i	0.032197-0.008050 i	0.048300-0.008050 i

Table 3. Fundamental quasinormal mode ($n = 0$) for Dirac field perturbations found by the 6th order WKB method with Padé approximants; $k = 0$, $\beta = 1$.

Therefore, from (3.2), we can obtain analytic expression for the position of the peak of the potential barrier

$$r_m = \frac{r_0}{\tan(r_0/3\beta)} + \mathcal{O}\left(\frac{1}{\ell}\right), \quad (8.3)$$

and, consequently for quasinormal modes using the expansion in terms of the inverse multiple number in the first order WKB formula

$$\omega = \frac{\sqrt{1 + 3\beta\gamma - 27k\beta^2}}{3\sqrt{3}\beta} \left(\ell + \frac{1}{2} - i \left(n + \frac{1}{2} \right) + \mathcal{O}\left(\frac{1}{\ell}\right) \right), \quad (8.4)$$

which generalizes the formula (19) of [76]. The latter can be obtained from (8.4) for $\gamma = 0$, $\beta = M$, and $k = \Lambda/3$.

The quasinormal modes in the eikonal limit (8.4) can be represented through the shadow radius (6.8) and Lyapunov exponent (6.10) as follows:

$$\omega = \frac{1}{R_s} \left(\ell + \frac{1}{2} \right) - i\lambda \left(n + \frac{1}{2} \right) + \mathcal{O}\left(\frac{1}{\ell}\right). \quad (8.5)$$

Let us note that the above eikonal formula applies only to the Schwarzschild branch of modes and does not account for the de Sitter and dark matter branches. Consequently, the correspondence between the eikonal quasinormal modes and null geodesics or shadows [77, 78] should be interpreted cautiously, keeping in mind that there are notable exceptions to this correspondence, particularly when higher curvature corrections or a cosmological constant are included [28–31]. Therefore, it remains uncertain whether this correspondence will

hold for gravitational perturbations in the Weyl theory, which lie beyond the scope of this investigation.

In the common range of applicability, we observe excellent agreement among all the methods. For instance, for $\ell = 1$ electromagnetic perturbations shown in Fig. 3, the time-domain integration and extraction of frequencies using the Prony method yield, for the Schwarzschild branch, $\omega M = 0.248270 - 0.092488i$, while the WKB method gives $\omega M = 0.248263 - 0.092488i$. Thus, the relative difference between the frequencies obtained by these two methods remains within a small fraction of one percent in this case.

9 Conclusions

The Weyl gravity suggests solutions to three interesting problems: (a) dark matter problem, without introducing dark matter fields, (b) reproducing the cosmological constant without formal introduction of it in the Lagrangian, (c) existence of traversable wormholes. The black-hole solution is not unique in this theory: For each value of the cosmological constant, the dark-matter term, and the asymptotic mass there is a one-parametric family of black-hole solutions obtained in [2], approaching the solutions of [1] when the additional parameter r_0 goes to zero. Moreover, the plethora of solutions in the Weyl theory include asymptotically de Sitter-like and anti-de Sitter black holes and wormholes.

In the present paper we have studied quasinormal spectrum of asymptotically de Sitter-like black holes and wormholes in the Weyl gravity. It was shown that the spectrum consists of the three branches of modes which dominate at different periods of time: Schwarzschild branch, dark matter branch and de Sitter branch. However, the limit of vanishing black hole mass is well defined only for the Mannheim-Kazanas black hole solution [1] and for this case we show that the modes of a black holes goes to those of the empty spacetime when mass goes to zero. The perturbation equations for the empty space in the Weyl gravity allow for an exact solution. Consequently, the quasinormal modes of the empty space in the Weyl gravity are obtained in the analytic form.

Quasinormal modes depend essentially on the parameters of the solutions responsible for the effective dark matter and cosmological terms, as well as on the parameter r_0 which distinguishes the three compact objects (Schwarzschild-like and non-Schwarzschild-like black holes, and a wormhole). In the eikonal limit we found the analytic expression for quasinormal frequencies, which respects the correspondence between quasinormal modes and null geodesics/radius of the shadow for all three branches.

In addition we have found the exact analytic expression for the radius of the shadow cast by the black hole or wormhole in the Weyl gravity.

Here we were limited by asymptotically de Sitter-like black holes. However, our analysis could in principle be extended to asymptotically anti-de Sitter spacetimes. For this case, quasinormal modes of vacuum spacetime is also expected to be the limit of black hole's frequencies, when the mass goes to zero [79].

Acknowledgments

A.K. is grateful to the Excellence Project FoS UHK 2204/2025–2026 for the financial support. A.Z. acknowledges the Research Centre for Theoretical Physics and Astrophysics at the Institute of Physics, Silesian University in Opava, for their hospitality.

References

- [1] Philip D. Mannheim and Demosthenes Kazanas. Exact Vacuum Solution to Conformal Weyl Gravity and Galactic Rotation Curves. *Astrophys. J.*, 342:635–638, 1989.
- [2] Petr Jizba and Kamil Mudruňka. Newman-Penrose formalism and exact vacuum solutions to conformal Weyl gravity. *Phys. Rev. D*, 110(12):124006, 2024.
- [3] Matt Visser. *Lorentzian wormholes: From Einstein to Hawking*. American Institute of Physics, 1995.
- [4] R. A. Konoplya and A. Zhidenko. Traversable Wormholes in General Relativity. *Phys. Rev. Lett.*, 128(9):091104, 2022.
- [5] Jose Luis Blázquez-Salcedo, Christian Knoll, and Eugen Radu. Traversable wormholes in Einstein-Dirac-Maxwell theory. *Phys. Rev. Lett.*, 126(10):101102, 2021.
- [6] Hans-Peter Nollert. TOPICAL REVIEW: Quasinormal modes: the characteristic ‘sound’ of black holes and neutron stars. *Class. Quant. Grav.*, 16:R159–R216, 1999.
- [7] Kostas D. Kokkotas and Bernd G. Schmidt. Quasinormal modes of stars and black holes. *Living Rev. Rel.*, 2:2, 1999.
- [8] R. A. Konoplya and A. Zhidenko. Quasinormal modes of black holes: From astrophysics to string theory. *Rev. Mod. Phys.*, 83:793–836, 2011.
- [9] R. A. Konoplya and C. Molina. The Ringing wormholes. *Phys. Rev. D*, 71:124009, 2005.
- [10] Thibault Damour and Sergey N. Solodukhin. Wormholes as black hole foils. *Phys. Rev. D*, 76:024016, 2007.
- [11] R. A. Konoplya and A. Zhidenko. Wormholes versus black holes: quasinormal ringing at early and late times. *JCAP*, 12:043, 2016.
- [12] Vitor Cardoso, Edgardo Franzin, and Paolo Pani. Is the gravitational-wave ringdown a probe of the event horizon? *Phys. Rev. Lett.*, 116(17):171101, 2016. [Erratum: *Phys.Rev.Lett.* 117, 089902 (2016)].
- [13] M. S. Churilova, R. A. Konoplya, and A. Zhidenko. Arbitrarily long-lived quasinormal modes in a wormhole background. *Phys. Lett. B*, 802:135207, 2020.
- [14] Mehrab Momennia and Seyed Hossein Hendi. Near-extremal black holes in Weyl gravity: Quasinormal modes and geodesic instability. *Phys. Rev. D*, 99(12):124025, 2019.
- [15] Mehrab Momennia and Seyed Hossein Hendi. Quasinormal Modes of Black Holes in Weyl Gravity: Electromagnetic and Gravitational Perturbations. *Eur. Phys. J. C*, 80(6):505, 2020.
- [16] Mehrab Momennia, Seyed Hossein Hendi, and Fatemeh Soltani Bidgoli. Stability and quasinormal modes of black holes in conformal Weyl gravity. *Phys. Lett. B*, 813:136028, 2021.
- [17] R. A. Konoplya. Conformal Weyl gravity via two stages of quasinormal ringing and late-time behavior. *Phys. Rev. D*, 103(4):044033, 2021.
- [18] Zainab Malik. Quasinormal modes of the mannheim–kazanas black holes. *Zeitschrift für Naturforschung A*, 79(11):1063–1073, 2024.
- [19] Ronald J. Riegert. Birkhoff’s Theorem in Conformal Gravity. *Phys. Rev. Lett.*, 53:315–318, 1984.
- [20] Tousif Islam. Globular clusters as a probe for Weyl Conformal Gravity. *Mon. Not. Roy. Astron. Soc.*, 488(4):5390–5399, 2019.
- [21] Koushik Dutta and Tousif Islam. Testing Weyl gravity at galactic and extra-galactic scales. *Phys. Rev. D*, 98(12):124012, 2018.

- [22] Keita Takizawa, Toshiaki Ono, and Hideki Asada. Gravitational lens without asymptotic flatness: Its application to the Weyl gravity. *Phys. Rev. D*, 102(6):064060, 2020.
- [23] Oğuzhan Kaşıkçı and Cemsinan Deliduman. Gravitational Lensing in Weyl Gravity. *Phys. Rev. D*, 100(2):024019, 2019.
- [24] Mohsen Fathi, Mona Kariminezhad, Marco Olivares, and J. R. Villanueva. Motion of massive particles around a charged Weyl black hole and the geodetic precession of orbiting gyroscopes. *Eur. Phys. J. C*, 80(5):377, 2020.
- [25] Mohsen Fathi, Marco Olivares, and J. R. Villanueva. Classical tests on a charged Weyl black hole: bending of light, Shapiro delay and Sagnac effect. *Eur. Phys. J. C*, 80(1):51, 2020.
- [26] Mohsen Fathi, Marco Olivares, and J. R. Villanueva. Gravitational Rutherford scattering of electrically charged particles from a charged Weyl black hole. *Eur. Phys. J. Plus*, 136(4):420, 2021.
- [27] Hao Xu and Man-Hong Yung. Black hole evaporation in Conformal (Weyl) gravity. *Phys. Lett. B*, 793:97–103, 2019.
- [28] R. A. Konoplya and Z. Stuchlík. Are eikonal quasinormal modes linked to the unstable circular null geodesics? *Phys. Lett. B*, 771:597–602, 2017.
- [29] R. A. Konoplya and A. F. Zinhailo. Quasinormal modes, stability and shadows of a black hole in the 4D Einstein-Gauss-Bonnet gravity. *Eur. Phys. J. C*, 80(11):1049, 2020.
- [30] S. V. Bolokhov. Black holes in Starobinsky-Bel-Robinson Gravity and the breakdown of quasinormal modes/null geodesics correspondence. *Phys. Lett. B*, 856:138879, 2024.
- [31] R. A. Konoplya. Further clarification on quasinormal modes/circular null geodesics correspondence. *Phys. Lett. B*, 838:137674, 2023.
- [32] Emanuele Berti, Vitor Cardoso, and Andrei O. Starinets. Quasinormal modes of black holes and black branes. *Class. Quant. Grav.*, 26:163001, 2009.
- [33] A. Lopez-Ortega. On the quasinormal modes of the de Sitter spacetime. *Gen. Rel. Grav.*, 44:2387–2400, 2012.
- [34] A. Lopez-Ortega. Dirac quasinormal modes of D-dimensional de Sitter spacetime. *Gen. Rel. Grav.*, 39:1011–1029, 2007.
- [35] R. A. Konoplya and A. Zhidenko. How general is the strong cosmic censorship bound for quasinormal modes? *JCAP*, 11:028, 2022.
- [36] R. A. Konoplya. Shadow of a black hole surrounded by dark matter. *Phys. Lett. B*, 795:1–6, 2019.
- [37] Kimet Jusufi, Mubasher Jamil, Paolo Salucci, Tao Zhu, and Sumarna Haroon. Black Hole Surrounded by a Dark Matter Halo in the M87 Galactic Center and its Identification with Shadow Images. *Phys. Rev. D*, 100(4):044012, 2019.
- [38] Xian Hou, Zhaoyi Xu, and Jiancheng Wang. Rotating Black Hole Shadow in Perfect Fluid Dark Matter. *JCAP*, 12:040, 2018.
- [39] Sourabh Nampalliwar, Sourabh Kumar, Kimet Jusufi, Qiang Wu, Mubasher Jamil, and Paolo Salucci. Modeling the Sgr A* Black Hole Immersed in a Dark Matter Spike. *Astrophys. J.*, 916(2):116, 2021.
- [40] Rui-Yan Chen, Faisal Javed, Dr. G. Mustafa, Sunil Kumar Maurya, and Saibal Ray. Dual effect of string cloud and dark matter halos on particle motions, shadows and epicyclic oscillations around Schwarzschild black holes. *JHEAp*, 44:172–186, 2024.
- [41] Reggie C. Pantig. Apparent and emergent dark matter around a Schwarzschild black hole. *Phys. Dark Univ.*, 45:101550, 2024.

- [42] Gabriel Gómez and Patrick Valageas. Constraining self-interacting scalar field dark matter from the black hole shadow of the Event Horizon Telescope. *Phys. Rev. D*, 109(10):103038, 2024.
- [43] Caio F. B. Macedo, João Luís Rosa, and Diego Rubiera-Garcia. Optical appearance of black holes surrounded by a dark matter halo. *JCAP*, 07:046, 2024.
- [44] Farook Rahaman, Ksh. Newton Singh, Rajibul Shaikh, Tuhina Manna, and Somi Aktar. Shadows of Lorentzian traversable wormholes. *Class. Quant. Grav.*, 38(21):215007, 2021.
- [45] Shinta Kasuya and Masataka Kobayashi. Throat effects on shadows of Kerr-like wormholes. *Phys. Rev. D*, 103(10):104050, 2021.
- [46] Salvatore Capozziello, Soroush Zare, Luis M. Nieto, and Hassan Hassanabadi. Modified Kerr black holes surrounded by dark matter spike. *arXiv:2311.12896*, 11 2023.
- [47] Volker Perlick and Oleg Yu. Tsupko. Calculating black hole shadows: Review of analytical studies. *Phys. Rept.*, 947:1–39, 2022.
- [48] Ziri Younsi, Alexander Zhidenko, Luciano Rezzolla, Roman Konoplya, and Yosuke Mizuno. New method for shadow calculations: Application to parametrized axisymmetric black holes. *Phys. Rev. D*, 94(8):084025, 2016.
- [49] Kirill A. Bronnikov, Roman A. Konoplya, and Thomas D. Pappas. General parametrization of wormhole spacetimes and its application to shadows and quasinormal modes. *Phys. Rev. D*, 103(12):124062, 2021.
- [50] R. A. Konoplya and A. Zhidenko. Shadows of parametrized axially symmetric black holes allowing for separation of variables. *Phys. Rev. D*, 103(10):104033, 2021.
- [51] Petya G. Nedkova, Vassil K. Tinchev, and Stoytcho S. Yazadjiev. Shadow of a rotating traversable wormhole. *Phys. Rev. D*, 88(12):124019, 2013.
- [52] Rajibul Shaikh. Shadows of rotating wormholes. *Phys. Rev. D*, 98(2):024044, 2018.
- [53] Takayuki Ohgami and Nobuyuki Sakai. Wormhole shadows. *Phys. Rev. D*, 91(12):124020, 2015.
- [54] Muhammed Amir, Kimet Jusufi, Ayan Banerjee, and Sudan Hansraj. Shadow images of Kerr-like wormholes. *Class. Quant. Grav.*, 36(21):215007, 2019.
- [55] M. S. Churilova, R. A. Konoplya, Z. Stuchlik, and A. Zhidenko. Wormholes without exotic matter: quasinormal modes, echoes and shadows. *JCAP*, 10:010, 2021.
- [56] Aurélien Barrau, Killian Martineau, Jeremy Martinon, and Flora Moulin. Quasinormal modes of black holes in a toy-model for cumulative quantum gravity. *Phys. Lett. B*, 795:346–350, 2019.
- [57] Oleksandr Stashko. Quasinormal modes and gray-body factors of regular black holes in asymptotically safe gravity. *Phys. Rev. D*, 110(8):084016, 2024.
- [58] Alexey Dubinsky and Antonina Zinhailo. Asymptotic decay and quasinormal frequencies of scalar and Dirac fields around dilaton-de Sitter black holes. *Eur. Phys. J. C*, 84(8):847, 2024.
- [59] A. F. Zinhailo. Quasinormal modes of Dirac field in the Einstein–Dilaton–Gauss–Bonnet and Einstein–Weyl gravities. *Eur. Phys. J. C*, 79(11):912, 2019.
- [60] Wei Xiong, Peng Liu, Cheng-Yong Zhang, and Chao Niu. Quasinormal modes of the Einstein–Maxwell–aether black hole. *Phys. Rev. D*, 106(6):064057, 2022.
- [61] Milena Skvortsova. Quasinormal Frequencies of Fields with Various Spin in the Quantum Oppenheimer–Snyder Model of Black Holes. *Fortsch. Phys.*, 72(9-10):2400132, 2024.
- [62] Milena Skvortsova. Ringing of Extreme Regular Black Holes. *Grav. Cosmol.*, 30(3):279–288, 2024.
- [63] Zainab Malik. Perturbations and Quasinormal Modes of the Dirac Field in Effective Quantum Gravity. *arXiv:2409.01561*, 9 2024.

- [64] Bilel Hamil and Bekir Can Lütfüoğlu. Schwarzschild black hole surrounded by a cloud of strings in the background of perfect fluid dark matter*. *Chin. Phys. C*, 49(2):025107, 2025.
- [65] Hang Liu and Hong Guo. Massive scalar perturbations and quasinormal modes of a rotating black hole in analog gravity. *Phys. Rev. D*, 110(10):104058, 2024.
- [66] R. A. Konoplya, A. Zhidenko, and A. F. Zinhailo. Higher order WKB formula for quasinormal modes and grey-body factors: recipes for quick and accurate calculations. *Class. Quant. Grav.*, 36:155002, 2019.
- [67] Sai Iyer and Clifford M. Will. Black Hole Normal Modes: A WKB Approach. 1. Foundations and Application of a Higher Order WKB Analysis of Potential Barrier Scattering. *Phys. Rev. D*, 35:3621, 1987.
- [68] R. A. Konoplya. Quasinormal behavior of the d-dimensional Schwarzschild black hole and higher order WKB approach. *Phys. Rev. D*, 68:024018, 2003.
- [69] Jerzy Matyjasek and Michał Opala. Quasinormal modes of black holes. The improved semianalytic approach. *Phys. Rev. D*, 96(2):024011, 2017.
- [70] Carsten Gundlach, Richard H. Price, and Jorge Pullin. Late time behavior of stellar collapse and explosions: 1. Linearized perturbations. *Phys. Rev. D*, 49:883–889, 1994.
- [71] Sean Fortuna and Ian Vega. Bernstein spectral method for quasinormal modes and other eigenvalue problems. *Eur. Phys. J. C*, 83(12):1170, 2023.
- [72] R. A. Konoplya and A. Zhidenko. Nonoscillatory gravitational quasinormal modes and telling tails for Schwarzschild–de Sitter black holes. *Phys. Rev. D*, 106(12):124004, 2022.
- [73] R. A. Konoplya and A. Zhidenko. Bernstein spectral method for quasinormal modes of a generic black hole spacetime and application to instability of dilaton–de Sitter solution. *Phys. Rev. D*, 107(4):044009, 2023.
- [74] M. S. Churilova and Z. Stuchlik. Ringing of the regular black-hole/wormhole transition. *Class. Quant. Grav.*, 37(7):075014, 2020.
- [75] Kirill A. Bronnikov and Roman A. Konoplya. Echoes in brane worlds: ringing at a black hole–wormhole transition. *Phys. Rev. D*, 101(6):064004, 2020.
- [76] A. Zhidenko. Quasinormal modes of Schwarzschild de Sitter black holes. *Class. Quant. Grav.*, 21:273–280, 2004.
- [77] Vitor Cardoso, Alex S. Miranda, Emanuele Berti, Helvi Witek, and Vilson T. Zanchin. Geodesic stability, Lyapunov exponents and quasinormal modes. *Phys. Rev. D*, 79(6):064016, 2009.
- [78] Kimet Jusufi. Quasinormal Modes of Black Holes Surrounded by Dark Matter and Their Connection with the Shadow Radius. *Phys. Rev. D*, 101(8):084055, 2020.
- [79] R. A. Konoplya. On quasinormal modes of small Schwarzschild-anti-de Sitter black hole. *Phys. Rev. D*, 66:044009, 2002.